Journal of The Electrochemical Society, **150** (4) A445-A454 (2003)
0013-4651/2003/150(4)/A445/10/$7.00 © The Electrochemical Society, Inc.

$LiPF_3(CF_2CF_3)_3$: A Salt for Rechargeable Lithium Ion Batteries

J. S. Gnanaraj,[a] M. D. Levi,[a,*] Y. Gofer,[a] D. Aurbach,[a,*,z] and M. Schmidt[b]

[a]*Department of Chemistry, Bar-Ilan University, Ramat-Gan 52900, Israel*
[b]*Merck KGaA, D-64293 Darmstadt, Germany*

$LiPF_3(CF_2CF_3)_3$ from Merck KGaA (LiFAP) was tested as a new electrolyte for Li-ion batteries that can replace the commonly used $LiPF_6$. The latter salt is known to be unstable, to decompose thermally to LiF and PF_5, and to readily undergo hydrolysis with protic species to form HF contamination in solutions. The latter contamination may have a detrimental impact on the performance of both anodes and cathodes for Li-ion batteries. Solutions comprising LiFAP, $LiPF_6$, and $LiN(SO_2CF_2CF_3)_2$ (LiBETI) in mixtures of ethylene, dimethyl, and diethyl carbonates were tested with composite graphite and $LiMn_2O_4$ electrodes. The tools for this study included voltammetry (fast and slow scan rates), chronopotentiometry, impedance spectroscopy, Fourier transform infrared, and X-ray and photoelectron spectroscopies. It was found that LiFAP is superior to $LiPF_6$ as an electrolyte for both graphite anodes and $LiMn_2O_4$ cathodes. This should be attributed to the different surface chemistry developed on these electrodes when $LiPF_6$ is replaced by LiFAP. An important impact of such a replacement is probably the absence of possible pronounced HF contamination in LiFAP solutions.
 [DOI: 10.1149/1.1557965]

Manuscript submitted May 13, 2002; revised manuscript received October 28, 2002. Available electronically February 28, 2003.

In recent years Li-ion batteries have become a commercial reality, and in the last few years we have seen increasing demands for these batteries for a large variety of applications.[1] We have also seen an increase in their mass production. The most common Li-ion battery systems include lithiated graphite anodes, $LiCoO_2$ (composite) cathodes, and electrolyte solutions based on an $LiPF_6$ salt in a mixture of alkyl carbonate solvents from the following list: ethylene carbonate, dimethyl carbonate, diethyl carbonate, ethyl-methyl carbonate, etc. (EC, DMC, DEC, EMC, respectively).[2] Li-ion batteries comprising these components can deliver several hundreds of charge discharge cycles at ambient temperatures and at high rates. For example, it may be possible to charge fully discharged Li-ion batteries to a maximal capacity within less than one hour.[3] Their temperature range may be between −30 and +60°C. However, as the temperature increases, their cycle life decreases and a capacity-fading upon cycling is recorded. In fact, the limited performance of Li-ion batteries at elevated temperatures (*e.g.*, >50°C) is one of their major drawbacks.[4]

In parallel to increasing mass production of Li-ion batteries, there are intensive R&D efforts throughout the world to further improve the performance of Li-ion battery technology. The major challenges are the improvement of high-temperature performance, minimizing capacity fading during prolonged operation (charge-discharge cycling), and replacing the $LiCoO_2$ cathode materials of the present Li-ion batteries by cheaper and more environmentally friendly materials such as $LiMn_2O_4$ (spinel) and its derivatives,[5] or $LiFePO_4$ (olivine).[6] A key factor that limits the performance of present Li-ion batteries and the possibility of using $LiMn_2O_4$ cathodes instead of $LiCoO_2$ relates to the salt that is commonly used in these battery systems, namely, $LiPF_6$. This salt may decompose spontaneously to LiF and PF_5.[7] The latter species react readily with protic substances (H_2O, ROH, surfaces with-OH groups such as glass) to form PF_yO_x compounds and HF.[8] Hence, HF is unavoidably present in all $LiPF_6$ solutions. This acidic contaminant is reduced on the lithiated graphite surfaces, reacts with protective surface films which are formed on the Li-C anodes, and also reacts with the Li_xMO_y cathode materials to form inactive phases on the surfaces of the cathode particles.[9] The presence of HF in solutions seems to induce the dissolution of cations of the transition metal of the cathode materials, which causes structural changes that lead to capacity fading.[10] Nevertheless, until recently $LiPF_6$ remained the best choice of an electrolyte for Li-ion batteries because all other relevant Li salts are less suitable: $LiAsF_6$ is poisonous (because of the arsenic), $LiClO_4$ may be explosive, $LiSO_3CF_3$ in solutions have too low a conductivity, and $LiN(SO_2CF_3)_2$ or $LiC(SO_2CF_3)_3$ may be too expensive. In the solutions of the latter two salts, the performance of both graphite anodes and Li_xMnO_y cathodes are not good enough due to insufficient passivation of the electrodes. $LiBF_4$ is also inferior to $LiPF_6$ due to the surface chemistry of graphite electrodes in the former salt solutions, which leads to insufficient passivation of lithiated graphite electrodes.[11]

Recently, Merck KGaA released information about a new salt, LiFAP-$LiPF_3(CF_2CF_3)_3$, developed by this company.[12] It is believed that replacing fluorine atoms of PF_6^- by $-CF_2CF_3$ groups stabilizes the anion. Hence, $PF_3(CF_2CF_3)_3^-$ is expected to be more stable than PF_6^-; therefore, it should not undergo hydrolysis as readily as PF_6^- or its decomposition product, PF_5, and thereby, LiFAP solutions should contain much less HF contamination than $LiPF_6$ solutions. In the present study, we compared the performance of LiFAP solutions in EC-DMC-DEC mixtures as electrolytes for Li-ion batteries with that of $LiPF_6$ solutions. $LiN(SO_2CF_2CF_3)_2$ (LiBETI) and $LiPF_6$-LiFAP (1:1) solutions were also studied to a limited extent. The electrodes of interest included platinum (an inert electrode for measuring the electrochemical window of the solutions), graphite, and $LiMn_2O_4$ (spinel). Standard electrochemical techniques have been used in conjunction with surface-sensitive techniques such as Fourier transform infrared (FTIR) and X-ray photoelectron spectroscopy (XPS).

Experimental

All the work was performed under a highly pure argon atmosphere in standard glove boxes from VAC, Inc. The anodes were composed of synthetic graphite (KS-6) from Timrex, Inc. (average particle size *ca.* 6 μm, 90 wt %), poly(vinylidene difluoride) (PVdF, 10 wt %) from Solvey, Inc., and copper foil current collectors. The cathodes were comprised of $LiMn_2O_4$ powder from Merck KGaA (particle size 5-10 μm, 75 wt %), 15 wt % graphite powder KS-6 (Timrex, Inc.) as a conductive additive, 5 wt % PVdF, 5 wt % conductive carbon black, and an aluminum foil (Goodfellow, England) current collector. Slurries containing the active mass and the binder were prepared using *N*-methyl pyrrolidone (Fluka, Inc.) and were coated on the appropriate current collectors, as already described.[13] The electrodes were dried in an oven at 140°C and were then transferred to the glove boxes. LiFAP, $LiPF_6$, LiFAP-$LiPF_6$

* Electrochemical Society Active Member.
z E-mail: aurbach@mail.biu.ac.il

1:1, and $LiN(SO_2CF_2CF_3)_2$ 1 M solutions in mixtures of EC-DEC-DMC (2:1:2 by volume) were obtained from Merck KGaA (highly pure, Li battery grade) and could be used as received. The HF and water content in solutions is currently measured at Merck. It is in the parts per million level for LiFAP and LiBETI solutions. The $LiPF_6$ solutions usually contain a few tens of ppm HF (may fluctuate between 10 and 100 ppm depending on unexpected possible exposure to moisture). All the electroanalytical characterizations of the electrodes were performed in three-electrode cells based on standard coin-type cells (model 2032, NRC Canada, ϕ 19 mm). A Li wire reference electrode was pasted on a nickel wire, which was placed between the working electrode and the Li counter-electrode foil, while being covered by the separator membrane (Celgard 2400). Long-term cycling tests done for graphite and $LiMn_2O_4$ electrodes were performed in two-electrode standard coin-type cells, separated by a porous polypropylene membrane (Celgard, Inc.) These cells were hermetically sealed in a dry air-filled glove box using the 2325 Coin Cell Crimper System (NRC/ICPET, Canada).

Beaker-type three-electrode cells were used for determining the electrochemical windows of the solutions and the basic voltammetric behavior of the solutions with noble metal electrodes using Pt wire electrodes. The cells contain polyethylene frames, which provide a parallel-plate configuration for the working and counter electrodes (Pt wire and Li foil, respectively).

Freshly prepared graphite electrodes usually had an open-circuit potential of *ca.* 3.3 V (*vs.* Li/Li^+). They were aged by voltammetric cycling between 3.0 and 0. V (*vs.* Li/Li^+) at $\nu = 1$ mV/s (three cycles). Li-ion intercalation-deintercalation processes were then studied in the potential range between 0.3 and 0 V (*vs.* Li/Li^+) by slow-scan-rate voltammetry (SSCV) and impedance spectroscopy (EIS).

Freshly prepared thin $LiMn_2O_4$ electrodes with open-circuit voltage (OCV) around 3.0 V (*vs.* Li/Li^+) were initially cycled four times (voltammetry) between 3.5 and 4.25 V (*vs.* Li/Li^+) at 1 mV/s before the rigorous electrochemical measurements. Prolonged galvanostatic cycling of all the various cells was performed at C/10 or C/4 rates in coin-type cells at 30°C in an incubator (Carbolite, Inc., model PIF30-200). For voltammetric measurements an Arbin, Inc., computerized multichannel battery tester and a computerized EG&G model 273 potentiostat were used. A Maccor multichannel system (model 2000) was used for prolonged galvanostatic cycling.

For surface analysis studies, we used a Magna 860 (Nicolet) FTIR spectrometer placed in a glove box under H_2O and CO_2-free atmosphere (fed by compressed air, treated with a Balston, Inc., air purifier). The electrodes were analyzed after electrochemical studies by diffuse reflectance mode (a DRIFT accessory from Harrick, Inc.), as already reported.[14] XPS characterization of electrodes was performed using the AXIS HS XPS spectrometer from Kratos Analytical, Inc. (England). The samples were transferred from the glove boxes to the spectrometer by a homemade transfer system that includes a gate valve and a magnetic manipulator from Norcal, Inc. (USA). This system ensures full protection from exposure to atmospheric contaminants. We also characterized surface films formed on gold mirrors and Pt foils that were polarized to low or high potentials in the various solutions by FTIR (external reflectance mode) and XPS.

Impedance spectra were measured using the Autolab model PGSTAT20 electrochemical system and a frequency response analyzer (FRA) from Eco Chemie B.V., Inc., driven by a Pentium II IBM PC. The amplitude of the ac voltage was 3 mV, and the electrodes were measured at a constant base potential after the appropriate equilibration as already described.[15]

Results and Discussion

Graphite electrodes.—Figures 1 and 2 compare the first three cyclic voltammograms (CVs) of Pt electrodes in $LiPF_3(CF_2CF_2)_3$ (LiFAP), $LiN(SO_2CF_2CF_3)_2$ (LiBETI), and $LiPF_6$ solutions, a-c, respectively. In Fig. 1, the potential was limited to the OCV (~3.3 V *vs.* Li/Li^+) to 0 V (Li/Li^+) range. As already discussed,[16] the relevant processes occurring in nonaqueous Li salt solutions with platinum electrodes include the following: bulk Li deposition below 0 V, bulk Li dissolution at ~0.55-0.6 V, Li under potential deposition (UPD) at ~0.65-0.7 V and 0.3-0.35 V (two peaks), stripping of UPD lithium at ~0.95-1.0 V and 1.3 V (two anodic peaks, corresponding to the cathodic Li UPD peaks), reduction of trace water at ~1.5 V, and a corresponding anodic process at ~1.8-2.0 V, which may be related to oxidation of hydrogen adsorbed to the platinum (formed by reduction of trace water). All the CV peaks of cathodic processes in the list are superimposed on a cathodic wave, which relates to reduction of both solvent molecules and salt anions at potentials below 2 V.[17] This cathodic wave is pronounced only during the first cathodic polarization of the electrode, since all the above-mentioned processes (except the Li deposition-dissolution ones) form insoluble surface species that passivate the electrodes (*e.g.*, $ROCO_2Li$ formed by solvent reduction, LiF formed by salt reduction, and LiOH formed by trace water reduction.)[16,17]

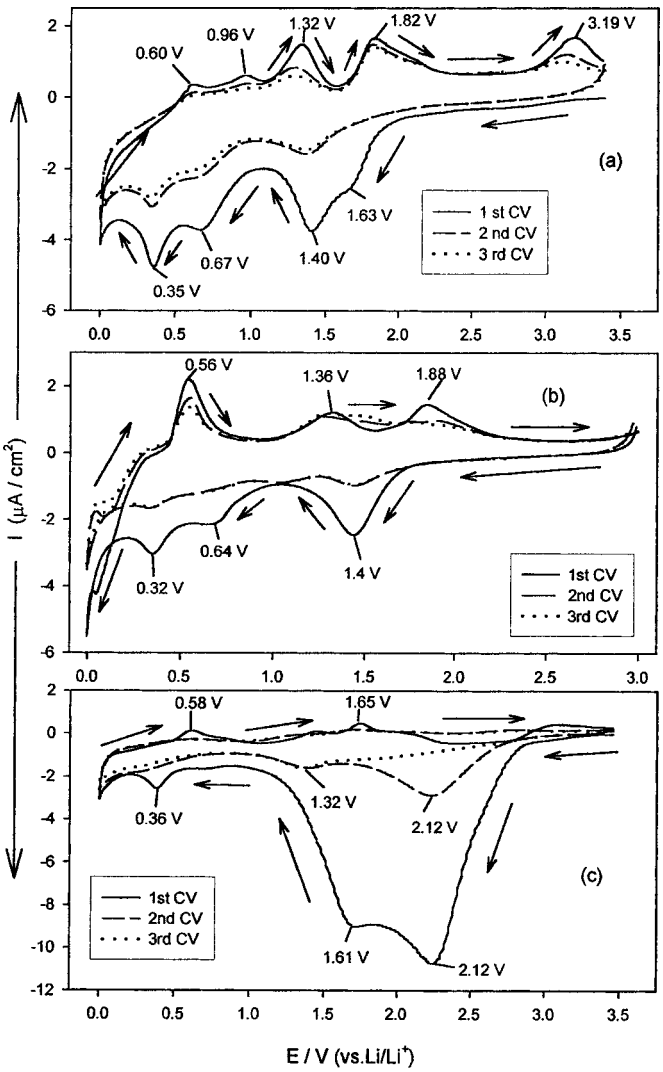

Figure 1. The first three CVs between OCV and 0 V at 30°C with Pt as working electrodes at 20 mV/s scan rate (lithium foil counter and reference electrodes): (a) EC:DEC:DMC 1 M LiFAP (<10 ppm water), (b) EC:DEC:DMC 1 M LiBETI (<10 ppm water), and (c) EC:DEC:DMC 1 M $LiPF_6$ (<10 ppm water).

This description fits the voltammograms related to the LiFAP and the LiBETI solutions presented in Fig. 1a and b. The voltammograms related to the $LiPF_6$ solutions are different (Fig. 1c), showing

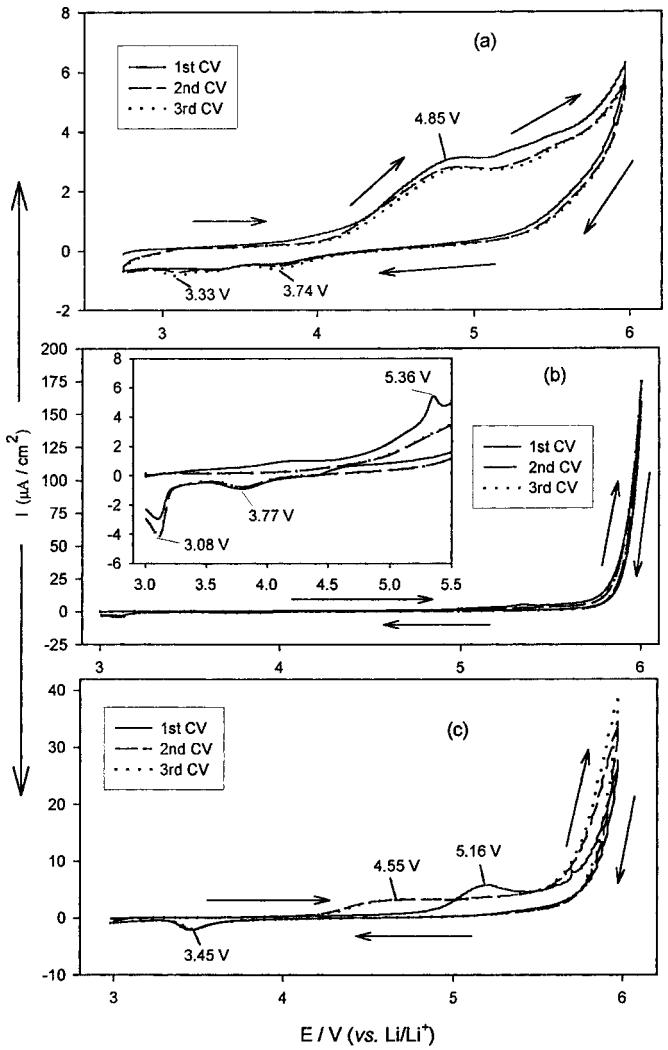

Figure 2. The first three CVs between OCV and 6 V at 30°C with Pt working electrodes at 20 mV/s scan rate (lithium as counter and reference electrodes): (a) EC:DEC:DMC 1 M LiFAP (<10 ppm water), (b) EC:DEC:DMC 1 M LiBETI (<10 ppm water), and (c) EC:DEC:DMC 1 M $LiPF_6$ (<10 ppm water).

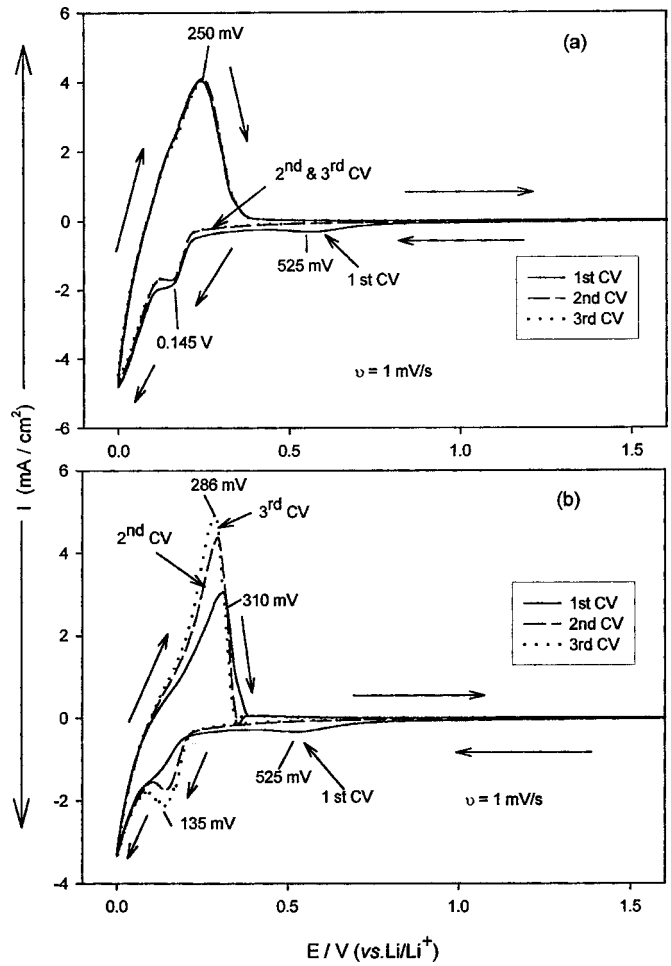

Figure 3. The first three CVs between OCV and 4.25 V at 30°C with graphite (KS6) working electrode at 1 mV/s scan rate (lithium as counter and reference electrodes): (a) EC:DEC:DMC 1 M LiFAP and (b) EC:DEC:DMC 1 M $LiPF_6$.

a pronounced, irreversible cathodic wave in the 2.5-1.5 V (Li/Li^+) range, which can be attributed to reduction of trace HF and PF_6^- anions.[18] As seen in Fig. 1c, the electrodes reach passivation in the $LiPF_6$ solution as well (the cathodic wave disappears upon consecutive CV cycling). The similarity in the voltammetric behavior of LiFAP and LiBETI solutions, which differs from the behavior of the $LiPF_6$ solutions, seems to indicate that the latter is contaminated by HF, and also that the PF_6^- anion may be more cathodically reactive than the other two anions (FAP^- and $BETI^-$).

Figure 2 relates to the anodic branch of the CV of Pt electrodes in the three solutions in the potential range 3-6 V (Li/Li^+). While the voltammetric behavior of Pt electrodes in the three solutions differs as far as the fine details are concerned, in general, there are some important similarities. Some low anodic currents can be measured at potentials between 4 and 5 V. At potentials above 5.5 V, the anodic (oxidation) currents measured intensify. The oxidation processes behind the anodic currents in Fig. 2 are irreversible and should be attributed to oxidation of solvent molecules and anions based on previous studies.[19,20] We attribute the anodic currents at potentials above 3 V in the CVs related to the LiFAP solutions to the possible unidentified impurities.

Figure 3 shows low-resolution (1 mV/s) CVs of graphite electrodes in LiFAP and $LiPF_6$ solutions (a, b, respectively). These CVs reflect the irreversible reduction of solution species at potentials below 2 V, which form passivating surface films (appearing only during the first cathodic wave), and the reversible lithium insertion and deinsertion processes at potentials below 0.20 V (cathodic) and above 0.15 V (anodic), respectively. It is important to note that the first and subsequent CVs related to the LiFAP solution are very similar in the Li insertion-deinsertion potential range (<0.3 V), while the CVs related to the $LiPF_6$ solution change upon repeated cycling and reach stability only after three to four subsequent cycles.

Figure 4 presents typical SSCVs measured with graphite electrodes in LiFAP and $LiPF_6$ solutions (a, b, respectively). Each figure shows two CVs, as indicated. One CV was measured after stabilization of the electrode (two to three consecutive CV cycles in the 0-3 V range), and the other one was measured after a week of measurements that included CV cycling. Both sets of CVs are typical of lithiation-delithiation cycles of graphite electrodes, clearly showing all four stages of Li intercalation into graphite, as already discussed.[21] However, it is very significant that the CVs related to the LiFAP solution are nearly identical, while the CVs related to the $LiPF_6$ solutions differ from each other in their anodic branches. The differences in the CVs in Fig. 4b show that in $LiPF_6$ solutions, there are long-term secondary processes that affect the electrode kinetics.

Figure 5 compares cycling data (capacity *vs.* cycle number curves) of graphite electrodes in four solutions containing the fol-

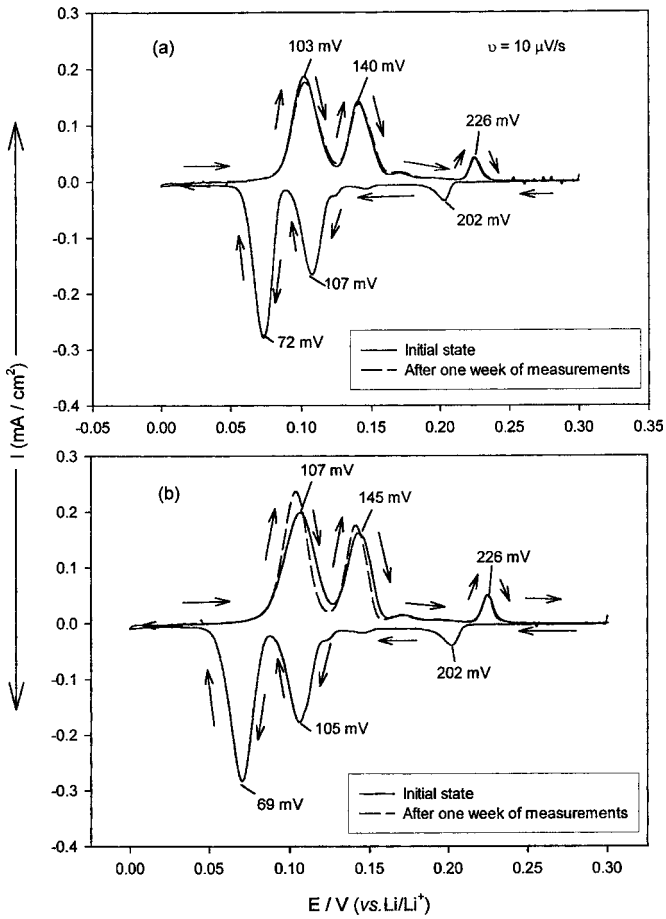

Figure 4. SSCVs between 0.3 and 0 V with graphite (KS6) as the working electrode at the scan rate of 10 μV/s (lithium as counter and reference electrodes): (a) EC:DEC:DMC 1 M LiFAP, (b) EC:DEC:DMC 1 M $LiPF_6$, (——) the SSCV of pristine electrodes, and (— — —) the SSCV measured after 1 week of measurements (cycling experiments at different rates at 30°C).

lowing Li salts (1 M solutions): LiFAP, $LiPF_6$, LiBETI, and LiFAP-$LiPF_6$ 1:1, as indicated. Both charge and discharge responses are presented (solid and dashed lines, as indicated, Li deinsertion-insertion processes, respectively). It is very significant that in the LiFAP solutions, the highest capacity and the best stability are achieved, while in the other solutions the capacity fading upon cycling is much more pronounced. In addition, comparing the charge and discharge curves related to the four systems, in LiFAP solutions, the electrodes reach stability much faster than in the other solutions. This finding correlates with the results presented in Fig. 3 and 4.

Figure 6 shows cycling data of graphite electrodes at 60°C. In these experiments, the electrodes were cycled more than a hundred Li insertion-deinsertion cycles at 30°C before the temperature was raised to 60°C. It should be noted that the electrodes cycled in the $LiPF_6$ solution failed at 60°C. The electrode in the LiBETI solution also shows a continuous capacity fading at 60°C. In the LiFAP solutions, the graphite electrode could be cycled 50 times at high capacity before the capacity deteriorated. The most stable behavior of graphite electrodes at elevated temperatures was obtained in solutions containing both LiFAP and $LiPF_6$, as seen in the figure. In fact, graphite electrodes could be charged-discharged at high capacity and low capacity fading even at 80°C in LiFAP-$LiPF_6$ solutions, while in the other solutions mentioned previously, the electrodes fail at such a high temperature.

Figures 7 and 8 show families of Nyquist plots measured at different equilibrium potentials (indicated) with stabilized graphite

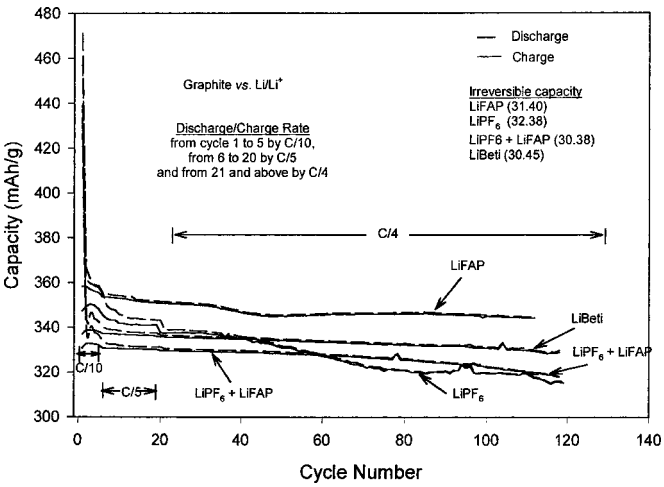

Figure 5. Typical cycle life curves (capacity *vs.* cycle number) of graphite electrodes obtained in coin-type cell testing at 30°C. Li metal counter electrodes, EC:DEC:DMC (2:1:2) 1 M LiFAP, $LiPF_6$, 0.5 M $LiPF_6$ + 0.5 M LiFAP, and LiBETI solutions as indicated in the figure. The current rates for the charge and the discharge processes are as indicated in the figure.

electrodes during lithium insertion in LiFAP and $LiPF_6$ solutions, respectively. The spectra include a high-medium, flat semicircle (more symmetrical with $LiPF_6$, and distorted with LiFAP solutions), and straight, linear Z'' *vs.* Z' behavior at the low frequency. At the very low frequencies, the Z'' *vs.* Z' lines become very steep. As already discussed in detail,[22] the high-medium frequency semicircles in these spectra relate to the surface films, which cover the graphite electrodes and their interface with the bulk carbon phase. The most important process related to the high-medium frequency impedance is Li-ion migration through the surface films[23] and the Li-ion transfer across the film-carbon interface, coupled with the relevant capacitances (related to the surface films and the double layer[24]). It should be noted that in some cases the time constants related to the surface films and the interfacial charge transfer are well separated, and hence, the impedance spectra show two high-medium frequency semicircles. In other cases, as in the present systems, the time constants are not separated. Therefore, the time constants related to the surface films appear as single flat semicircles. At

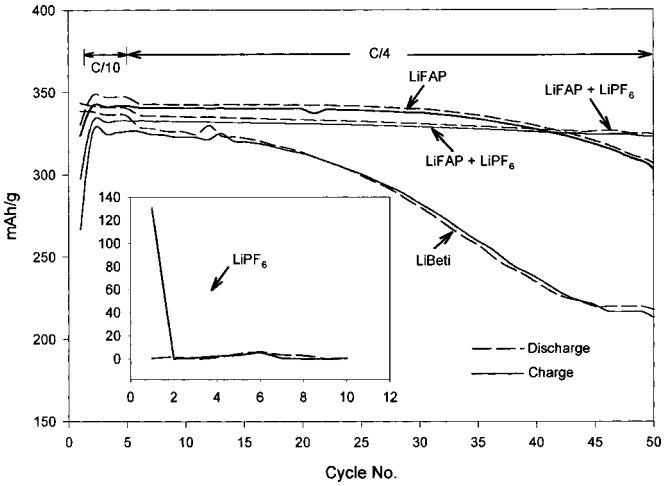

Figure 6. Typical cycle life (capacity *vs.* cycle number) of graphite electrodes obtained in coin-type cell at 60°C after about 120 cycles at 30°C. Li metal counter electrodes, EC:DEC:DMC (2:1:2) 1 M LiFAP, 0.5 M $LiPF_6$ + 0.5 M LiFAP, 1 M LiBETI and 1 M $LiPF_6$ (insert) solutions (as indicated in the figure). The rates for the charge and the discharge processes are also indicated in the figure.

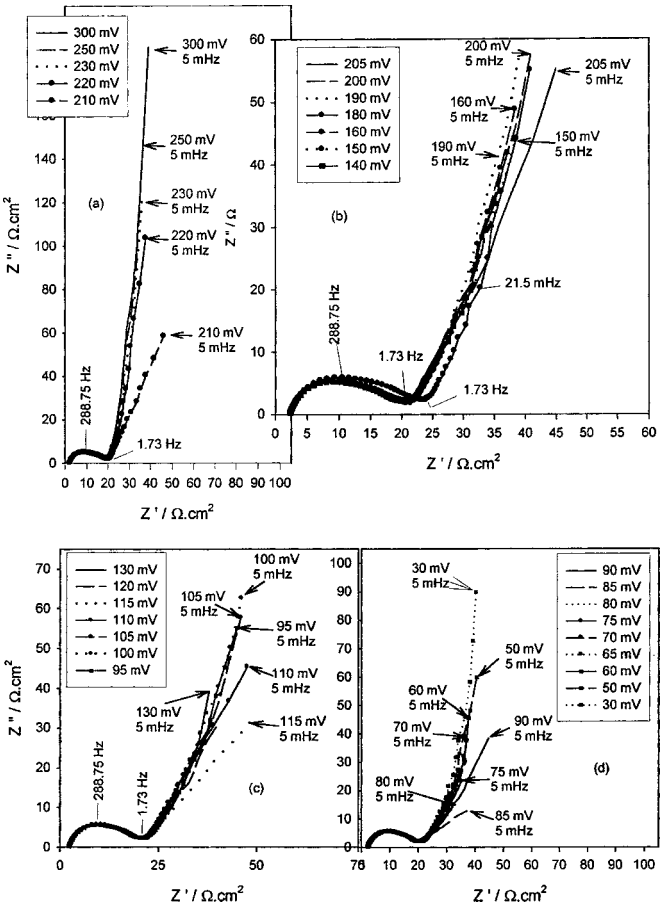

Figure 7. A family of Nyquist plots obtained from graphite, KS6 electrodes at different equilibrium potentials in EC:DEC:DMC (2:1:2) 1 M LiFAP solutions at 30°C. These series of experiments were carried out after the electrodes were cycled (CV) in the potential range of interest, during which its surface chemistry was established. Some frequencies are also marked near the spectra. The relevant potentials are indicated.

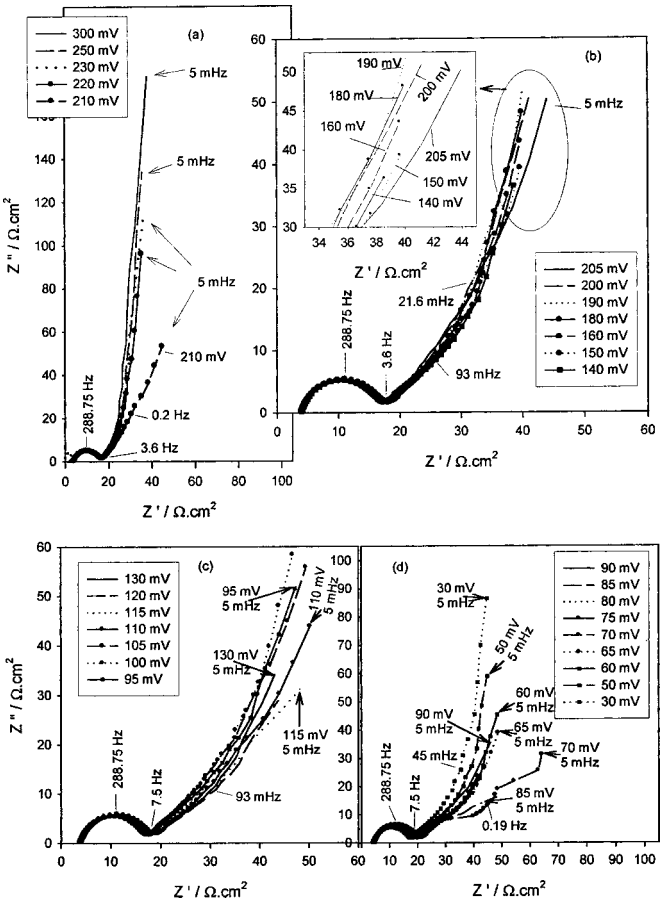

Figure 8. Same as Fig. 7 in EC:DEC:DMC (2:1:2) 1 M $LiPF_6$ solutions.

the low frequencies, the straight Z'' *vs.* Z' lines (see Fig. 7 and 8) behave as ''Warburg''-type elements, and reflect solid-state diffusion of Li ions in the bulk graphite. The chemical diffusion coefficient of Li ions in graphite as a function of potential and intercalation level can be calculated from this part of the impedance spectra.[22,23] At the very low frequencies, the steep, straight Z'' *vs.* Z' plots show a nearly capacitive behavior, thus reflecting the accumulation of lithium in the graphite via phase transitions between Li intercalation stages. The differential capacity of the electrode as a function of potential can be calculated from this domain of the impedance spectra (*i.e.*, curves similar to the CVs presented in Fig. 4 can be obtained from the EIS at very low frequencies.[22] It is very significant that the diameters of the semicircle in the Nyquist plots related to the LiFAP solution (Fig. 7) are higher than those of the semicircles in Fig. 8 ($LiPF_6$ solutions), *i.e.*, the surface impedance of graphite electrodes in LiFAP solutions is higher than that measured in $LiPF_6$ solutions. The impedance of both Li and lithiated graphite is usually higher in $LiPF_6$/alkyl carbonate solutions than that measured in alkyl carbonate solutions with salts such as $LiAsF_6$, $LiClO_4$, $LiC(SO_2CF_3)_3$, etc.[11,24] This is because surface films formed on lithium and lithiated graphite electrodes in $LiPF_6$ solutions contain a high concentration of LiF formed by the reactions of both trace HF and PF_6^- anions on the active surfaces.[11,24] Surface films comprising LiF are highly resistive to Li-ion migration, much more than the surface films comprising organic or inorganic Li carbonates, which are formed by the reduction of the alkyl carbonates (in cases where the Li or Li-C surface chemistry is dominated by solvent reduction). Based on information from Merck KGaA, it is clear that LiFAP solutions contain much less HF than $LiPF_6$ solutions, and therefore, the surface films formed on lithiated graphite in the former solutions should contain less LiF, and hence should be less resistive than the surface films formed on graphite electrodes in the $LiPF_6$ solutions. Therefore, the impedance spectra in Fig. 7 and 8 that reflect a higher surface resistance of the graphite electrodes in the LiFAP solutions may indicate some involvement of the FAP^- anion in the surface chemistry of the graphite electrodes in a way that stabilizes the electrode-solution interface, as is evident from the high performance of Li-graphite electrodes in the LiFAP solutions, but also increases the impedance of the surface films. Therefore, it was very important to explore the surface chemistry of lithiated graphite electrodes in these solutions in order to understand the effect of LiFAP on the electrode's behavior. XPS and FTIR spectroscopy were used for that purpose.

We studied the surface chemistry of both graphite electrodes after cycling in solutions and Pt electrodes polarized cathodically in solutions to low potentials. Based on previous studies, similar surface films are formed on Li, Li-C, and noble metal electrodes polarized to low potentials in Li salt (nonaqueous) solutions.[25,26] However, the identification of surface species formed on noble metals is the easiest (due to the high resolution of the spectra obtained), and it opens the door to understanding the surface chemistry of the much more complicated composite, graphite electrodes.

Figure 9 compares XPS spectra of Pt electrodes polarized to low potentials in LiFAP, $LiPF_6$, and LiBETI solutions, as indicated. The most pronounced element on the electrode's surface treated in the $LiPF_6$ solutions is fluorine, which belongs to LiF (a typical peak at ~685-686 eV[27]). The carbon spectrum of the electrode treated in

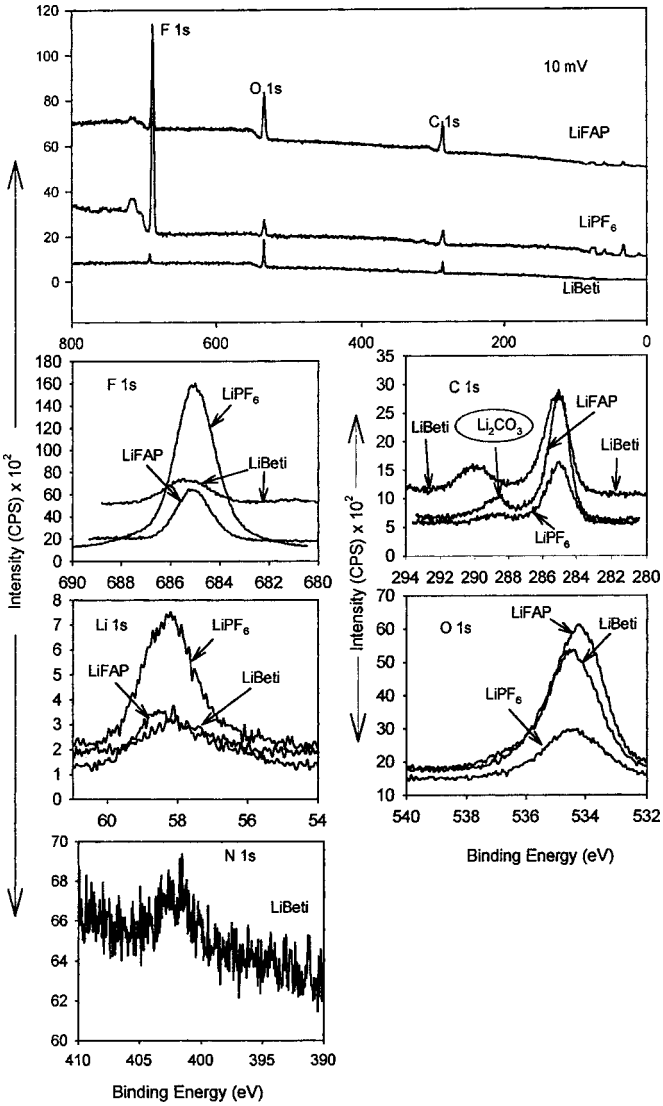

Figure 9. XPS spectra measured from Pt electrodes after cathodic polarization to 10 mV *vs.* Li/Li^+ for 3 h in LiFAP, LiBETI, and $LiPF_6$ solutions as indicated.

the LiFAP solution contains a broad peak at ~287-285 eV, which may relate to alkoxy species.[27] It is very significant that the carbon spectrum of this electrode does not contain carbonate peaks at high binding energies (>290 eV[27]). In contrast, the carbon spectra of the Pt electrodes treated in both LiFAP on LiBETI solutions contain carbonate carbons that reflect the formation of surface films originating from reduction of solvent molecules (alkyl carbonates are reduced to $ROCO_2Li$ species[11,24-26]). The lithium and fluorine peaks in the spectra of the electrodes treated in LiFAP and BETI are much smaller than those peaks in the spectrum related to the $LiPF_6$ solution, while the oxygen peak in the spectra related to the former solutions is pronouncedly higher compared with the O 1s spectrum related to the $LiPF_6$ solution. We do not show the results of peak convolutions and more rigorous peak analysis, because such a treatment has already been described in detail,[28] and in fact, the surface chemistry reflected from the spectra in Fig. 9 is well known and understood.[11,24-26,28,29] The main message of the spectral studies summarized in Fig. 9 is that in LiFAP solutions the surface chemistry is dominated by solvent reduction. This is in contrast to the case of $LiPF_6$ solutions in which direct reduction of trace HF and a possible secondary reaction of HF with solvent reduction products

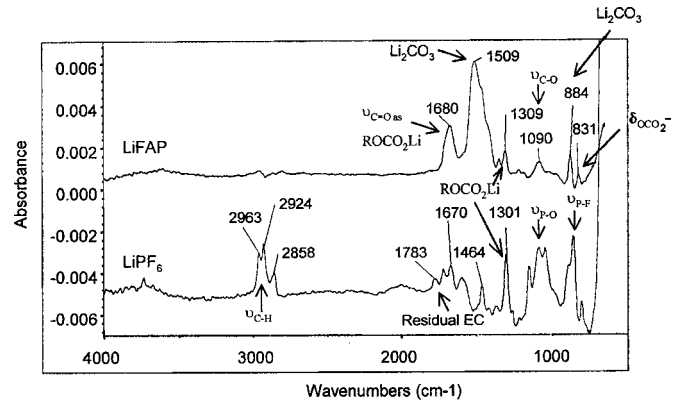

Figure 10. FTIR spectra (grazing angle reflectance mode) measured *ex situ* from high reflective gold electrodes after being polarized cathodically to 300 mV *vs.* Li/Li^+ for 3 h in $LiPF_6$ and LiFAP electrolyte solutions (indicated).

(*e.g.*, $ROCO_2Li + HF \rightarrow ROCO_2H + LiF$), as already described,[30] have a very strong impact on the electrodes surface chemistry in a way that makes LiF a major surface species in the passivating surface films.

Figure 10 shows FTIR spectra obtained from gold mirrors (coated on glass) which were polarized cathodically to 300 mV (Li/Li^+) in LiFAP and $LiPF_6$ solutions (*ex situ*, external reflectance mode).[31] It is very significant that the spectra of Fig. 10 differ considerably from each other. Spectrum 10a, related to the LiFAP solution, is typical of a mixture of $ROCO_2Li$ species [*e.g.*, the major EC reduction product, $(CH_2OCO_2Li)_2$],[31] and Li_2CO_3 are marked. The analysis of spectrum 10a is based on previous intensive work.[15,16,24-26,30,31] Spectrum 10b, related to the $LiPF_6$ solution, is more complicated than spectrum 10a. It contains pronounced ν_{CH} peaks in the 2850-2970 cm^{-1} range, some C = O (carbonyl) peaks in the 1800-1600 cm^{-1} range, $\delta_{C\text{-}H}$ peaks at ~1450-1400 cm^{-1}, a peak at ~1300 cm^{-1} that can be attributed to organic carbonate groups,[32] and a pronounced peak at ~850 cm^{-1}, which should be attributed to $\nu_{P\text{-}F}$ bands.[11] Based on previous studies,[11,15,16,24-26,30,31,33] spectrum 10b belongs to a mixture of $ROCO_2Li$ species (*e.g.*, 1670 and 1301 cm^{-1} carbonyl peaks) and ROLi species (*e.g.*, the 2970-2850 cm^{-1} $\nu_{C\text{-}H}$ peaks, the 1460 cm^{-1} $\delta_{C\text{-}H}$ peaks, and the 1150-1000 cm^{-1} $\nu_{C\text{-}O}$ peaks), which are typical alkyl carbonate reduction products,[11,24-26] and also to Li_xPF_y and Li_xPOF_y species, which are reduction products of PF_6^- and PF_3O. The latter species is a hydrolysis product of the PF_6^- anion. It is clear from the spectra of Fig. 10 that in LiFAP solutions, the surface films formed on noble metals polarized to low potentials are dominated by organic and inorganic carbonates, while in $LiPF_6$ solutions, the surface films on noble metals are dominated by salt reduction products and alkoxy species. The results from the FTIR measurements correlate well with the XPS data presented in Fig. 9. Spectral studies of graphite electrodes treated in these solutions were in line with the results presented in Fig. 9 and 10. It is clear from these spectral studies that replacement of $LiPF_6$ by LiFAP in alkyl carbonate solutions changes the surface chemistry of the lithiated graphite electrodes.

As explained previously, in $LiPF_6$ solutions, the high reactivity of the PF_6^- anion and the trace HF plays a major role. In LiFAP solutions, the formation of surface carbonates dominates the electrode surface chemistry, since there is no high HF contamination that removes them from the surface in secondary reactions. The difference in the surface chemistry in LiFAP and $LiPF_6$ solutions may explain the difference in the behavior of graphite electrodes in the two solutions, as presented in Fig. 1-8. However, the spectral studies could not provide any information about the possible in-

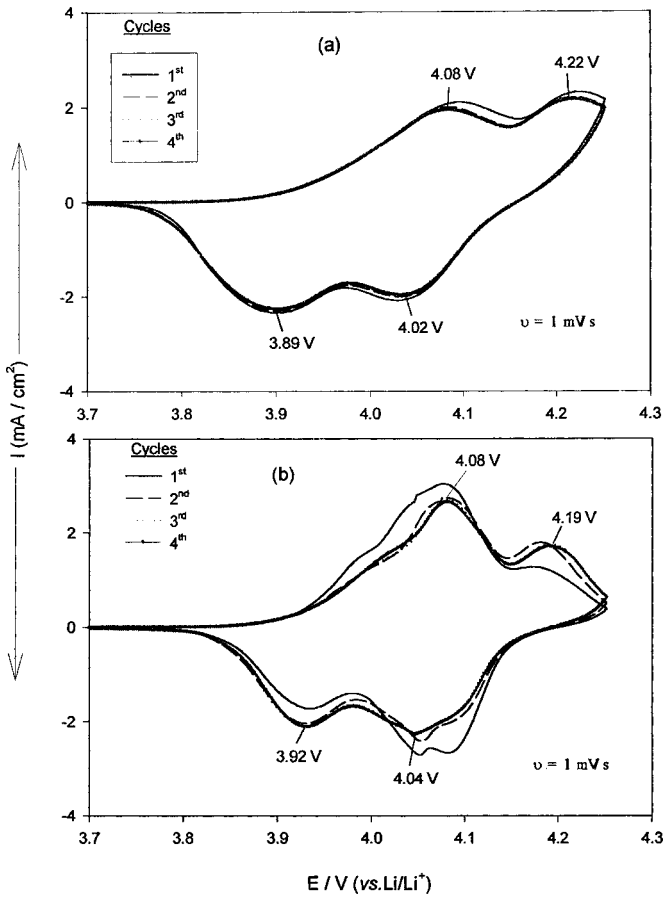

Figure 11. First four consecutive CVs of $LiMn_2O_4$ electrodes between 3.7 and 4.25 V at a scan rate of 1 mV/s (lithium as counter and reference electrodes): (a) EC:DEC:DMC (2:1:2) 1 M LiFAP and (b) EC:DEC:DMC 1 M $LiPF_6$.

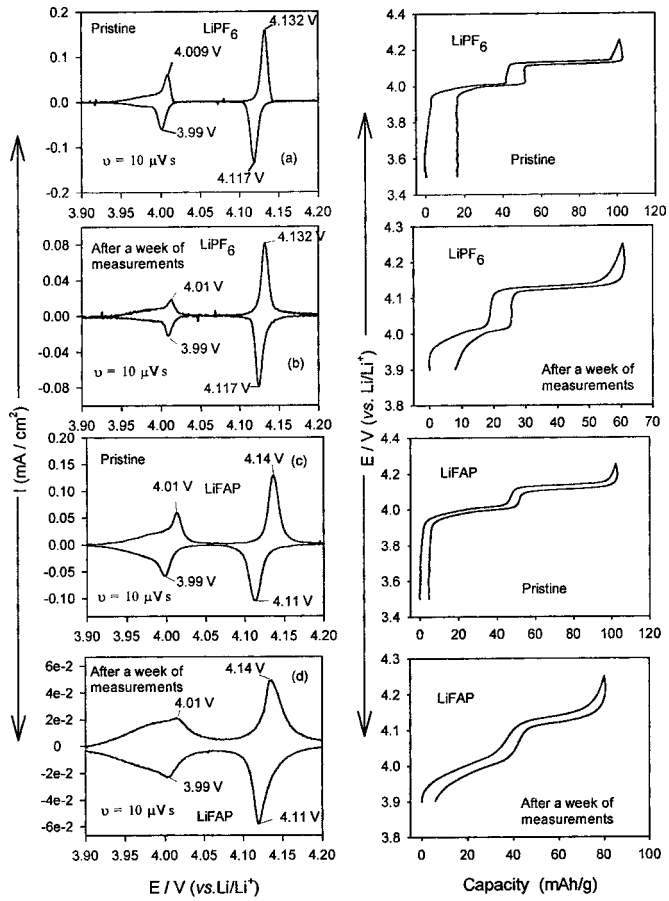

Figure 12. Left column: SSCVs of $LiMn_2O_4$ electrodes between 3.7 and 4.25 V at a scan rate of 10 μV/s (lithium as counter and reference electrodes) in EC:DEC:DMC 1 M $LiPF_6$ solutions (a) before and (b) after 1 week of measurements (cycling tests at different regions) and in EC:DEC:DMC 1 M LiFAP solutions (c) before and (d) after 1 week of measurements at 30°C. Right column: the corresponding electrode capacities (mAh/g) calculated from the CVs plotted *vs.* potential (Li/Li^+).

volvement of the FAP^- anion in the electrode surface chemistry and in the buildup of surface films, as would be expected from the impedance studies discussed (Fig. 7 and 8). Hence, the question about the possible reactivity of LiFAP on the electrode surfaces remains unanswered.

$LiMn_2O_4$ (spinel) electrodes.—Figure 11 shows four consecutive CVs measured with composite $LiMn_2O_4$ electrodes in LiFAP and $LiPF_6$ solutions (a and b, respectively). The CVs of Fig. 11 were measured at a relatively high potential scan rate for solid-state diffusion-controlled systems. Nevertheless, they show the expected two sets of peaks of Li insertion-deinsertion processes of these electrodes, which occur via phase transitions.[34] The two sets of CVs in Fig. 11 show two major differences:

1. The four consecutive CVs related to the LiFAP solution are very similar to each other. Stabilization occurs in the second cycle. In contrast, there are pronounced differences in the first three consecutive CVs related to the $LiPF_6$ solutions.

2. The hysteresis in the two pairs of CV peaks for the LiFAP solution (*e.g.*, the potential difference between the corresponding anodic and cathodic peak potentials) is much higher than that seen in the CVs related to the $LiPF_6$ solution. This difference in hysteresis relates to a difference in the kinetics of the electrodes in the two solutions.

Figure 12 shows SSCVs, (10 μV/s) of composite $LiMn_2O_4$ electrodes in LiFAP and $LiPF_6$ solutions (a, b and c, d, respectively) before and after 1 week of measurements at 30°C, which included different modes of charge-discharge cycling (a, c and b, d, respectively). In the right column, the capacity *vs.* potential is calculated from the CVs. The CVs in this figure reflect the highly reversible behavior of the $LiMn_2O_4$ electrodes in both solutions. The two Li insertion-deinsertion processes occurring at ~4.0 V and 4.12 (Li/Li^+) via first-order phase transitions are clearly seen. In addition, upon cycling at 30°C, a capacity fading is measured in both solutions. However, there are two major differences in the electrochemical behavior of the $LiMn_2O_4$ electrodes in the two solutions, as clearly demonstrated in Fig. 12: (*i*) the electrodes' capacity is higher in the LiFAP solutions and (*ii*) the electrodes' kinetics are more sluggish in the LiFAP solutions, as is evident from the broader peaks in Fig. 12c and d. Hence, the slow-scan-rate voltammetric behavior presented in Fig. 12 correlates well with the data in Fig. 11.

Figure 13 presents cycling data of $LiMn_2O_4$ electrodes at 30°C (repeated galvanostatic delithiation-lithiation cycles at C/10 rates). In general, some capacity fading was observed for these electrodes upon cycling, as is usually found for $LiMn_2O_4$ electrodes.[35] The capacity obtained in the LiFAP solutions is higher than that obtained with $LiPF_6$ solutions.

Figures 14 and 15 show Nyquist plots measured with stabilized $LiMn_2O_4$ composite electrodes during delithiation at several equilibrium potentials (indicated) in LiFAP and $LiPF_6$ solutions, respectively. In general, the impedance spectra of these electrodes in both solutions reflect the serial nature of Li insertion-deinsertion processes into $LiMn_2O_4$ electrodes, as already demonstrated and dis-

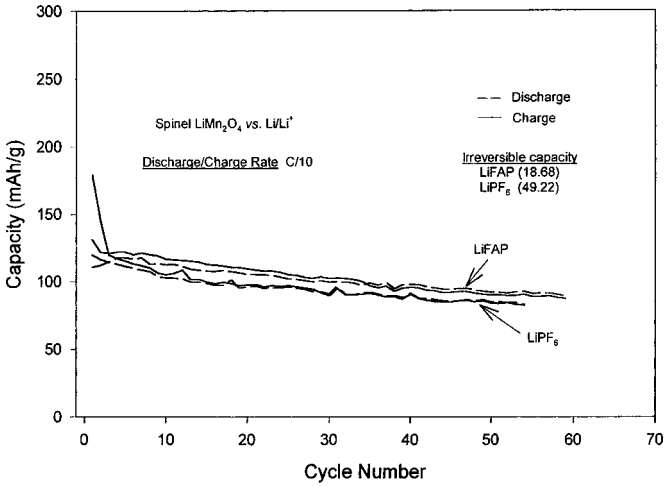

Figure 13. Typical cycle life curves (capacity *vs.* cycle number) of $LiMn_2O_4$ electrodes obtained at 30°C in coin-type cells (galvanostatic mode). Li metal counter electrodes, EC:DEC:DMC (2:1:2) 1 M LiFAP and 1 M $LiPF_6$ solutions as indicated. The rates for charge and discharge as indicated in the figure.

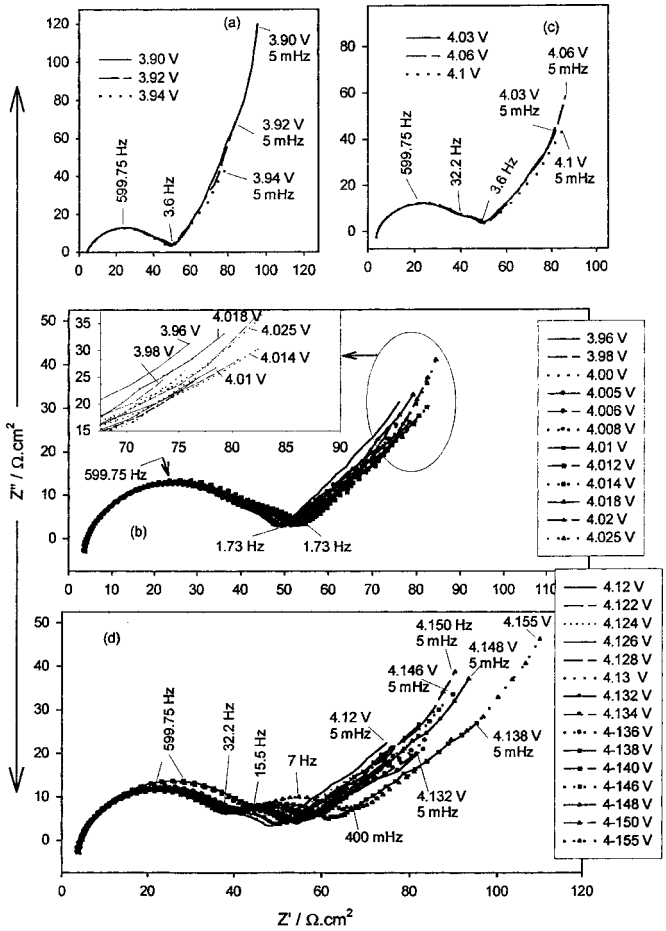

Figure 14. A family of Nyquist plots measured from $LiMn_2O_4$ electrodes in three-electrode coin-type cells in EC:DEC:DMC (2:1:2) 1 M LiFAP solutions at 30°C. The electrodes were preliminarily equilibrated at different potentials (as indicated) for at least 2-5 h before the EIS measurements.

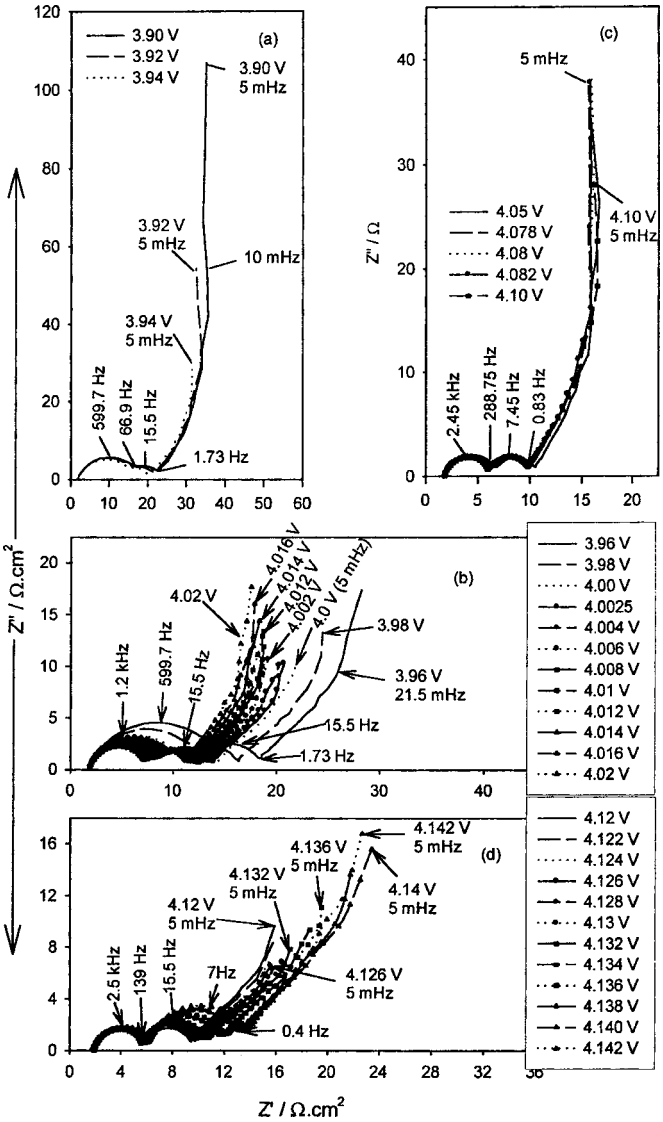

Figure 15. Same as Fig. 14, in EC:DEC:DMC (2:1:2) 1 M $LiPF_6$ solutions.

cussed in detail.[36] At the high-medium frequencies, two flat semicircles, which may be well separated (as in Fig. 15, $LiPF_6$ solutions) or superimposed (LiFAP solutions, Fig. 14), reflect Li migration through surface layers (the high-frequency semicircle) and interfacial charge transfer (the medium semicircle). At the low frequencies, a "Warburg"-type element (linear Z'' *vs.* Z' behavior) in the spectra reflect the solid-state diffusion of Li ions into the bulk $LiMn_2O_4$ particles. Finally, at the very low frequencies, the Nyquist plots behave as very steep Z'' *vs.* Z' straight lines that reflect the electrodes' capacitive behavior, namely, accumulation of charge due to delithiated Li or lithiation. A comparison between the families of spectra in Fig. 14 and 15 clearly demonstrates that the electrode impedance in $LiMn_2O_4$ is higher in LiFAP solutions, and the resolution of the spectra related to LiFAP solutions in the high-to-medium frequencies is lower. This means that the surface chemistry of the electrodes in both solutions is different, and hence, deserves special study. The higher impedance of the electrodes in the LiFAP solutions correlates well with their more sluggish kinetics, as reflected by the voltammetric studies (Fig. 11 and 12). The surface chemistry that can be developed in the various solutions was studied mainly with platinum electrodes polarized to high potential, because the *ex situ* study of composite $LiMn_2O_4$ electrodes by XPS or FTIR spectroscopy is highly problematic, especially when the focus is on the effects of the

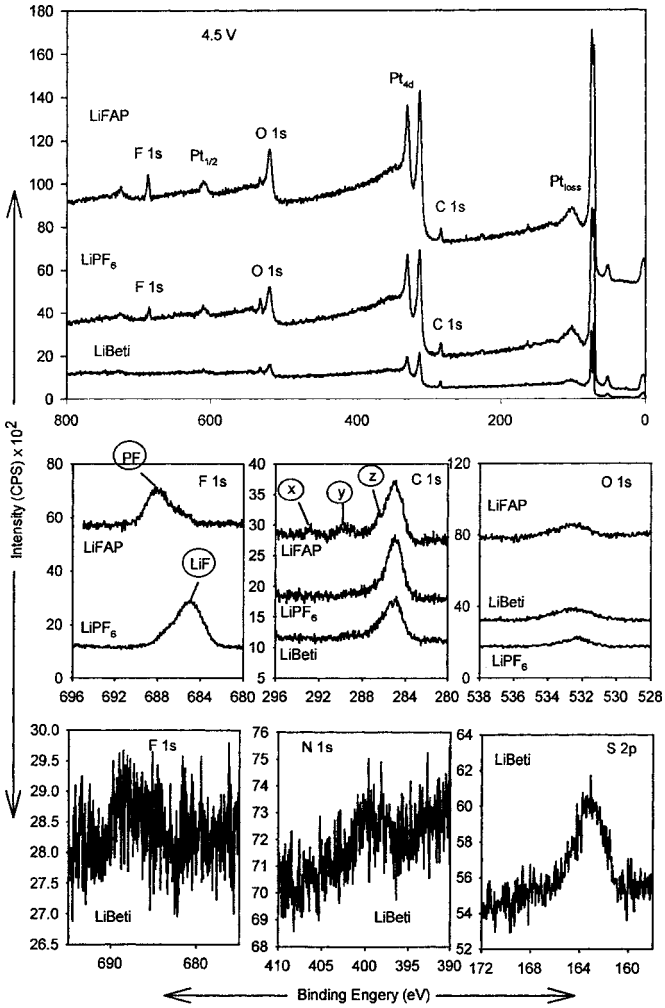

Figure 16. XPS data obtained from Pt electrodes polarized anodically to 4.5 V (for 3 h) in LiFAP, LiBETI, and $LiPF_6$ solutions as indicated.

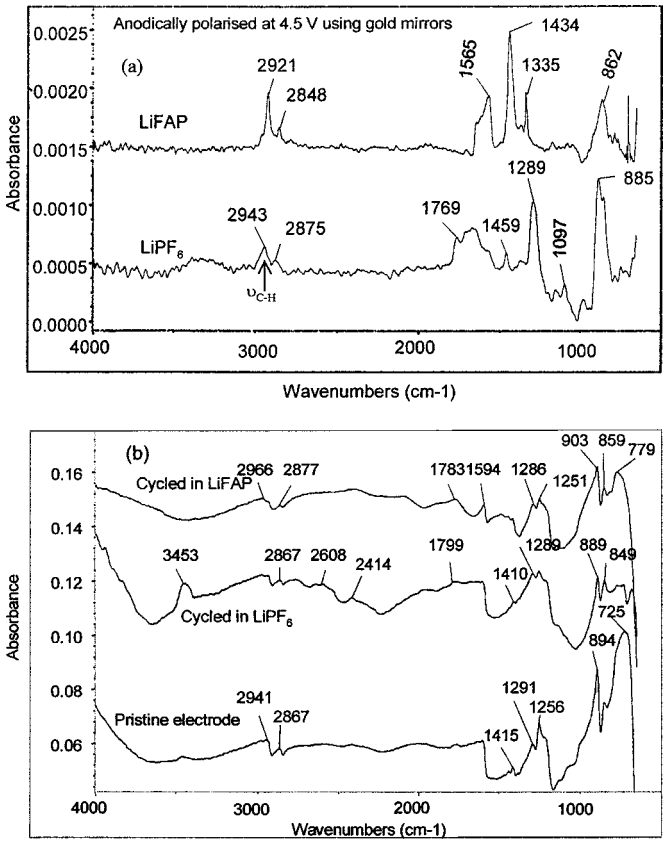

Figure 17. (a) FTIR spectra measured from highly reflective gold electrodes (grazing angle reflectance mode) polarized anodically to 4.5 V (Li/Li^+) in LiFAP and $LiPF_6$ solutions (indicated). (b) FTIR spectra measured from $LiMn_2O_4$ electrodes in diffuse reflectance mode (powders scraped from electrodes). The spectra of a pristine electrode and electrodes cycled in LiFAP and $LiPF_6$ solutions are indicated.

salt (*e.g.*, it may be very difficult to wash out residual salt from the porous composite electrodes, which reduces the reliability of the measurements).

Figure 16 compares XPS spectra of platinum electrodes polarized to 4.5 V (Li/Li^+) in LiFAP, $LiPF_6$, and LiBETI solutions. Although we did not study the electrochemical behavior of $LiMn_2O_4$ electrodes in LiBETI solutions, it was interesting to explore the surface chemistry developed at high potentials in the latter solutions as an example of HF-free situations. It is significant that the electrode treated in the $LiPF_6$ solution developed surface LiF, while the electrode treated in the LiFAP solution does not show a LiF peak but rather peaks of other F-containing species that probably originate from some (yet unidentified) reactions of the FAP^- anion.

Figure 17a shows FTIR spectra (external reflectance mode) of Pt electrodes polarized to 4.5 V in LiFAP and $LiPF_6$ solutions (indicated). The two spectra are definitely different from each other and contain typical pronounced peaks of organic species at around 2920-2850 cm^{-1} (ν_{CH}), 1800-1600 cm^{-1} ($\nu_{C=O}$), and 1450-1350 cm^{-1} (δ_{C-H}). The peaks at ~885-850 cm^{-1} may be attributed to species with P-F bonds. These spectra may reflect polymerization of the solvent molecule to derivatives of polyethylene oxide and polycarbonates, as already suggested.[37] Figure 17b (bottom) shows FTIR spectra of much lower resolution, obtained by diffuse reflectance mode, from powders scraped from a pristine $LiMn_2O_4$ electrode, and $LiMn_2O_4$ electrodes cycled in LiFAP and $LiPF_6$ solutions, as indicated. The spectrum of the pristine electrode reflects the PVdF binder and possible surface groups on the carbon additives. The other two spectra are somewhat richer in peaks and may indeed reflect possible precipitation of organic species on the electrode surface. The spectra related to LiFAP and $LiPF_6$ solutions are also different. However, it is impossible to use these spectra for any identification of surface films. Their importance lies in the fact that they reflect the difference in the surface chemistry of the electrodes, which is due only to the different electrolyte used. The difference in surface chemistry explains the difference in the electrochemical behavior of the electrodes in the LiFAP and $LiPF_6$ solutions. It is clear that in the $LiPF_6$ solution, surface LiF is formed. In contrast to graphite electrodes where there is a constant driving force toward the formation of LiF, in the case of the cathode materials, LiF may be formed in thin layers by decomposition of the salt to LiF and PF_5 on the cathode and/or by acid-base reactions between $LiMn_2O_4$ and HF. A sufficiently thin LiF layer may not impede Li-ion transport to the active mass, yet may inhibit to some extent the reaction of solvent molecules on the cathode material. However, other reactions between the active mass and species such as trace HF, which are unavoidably present in $LiPF_6$ solutions, may have a detrimental effect on the electrode's overall capacity. In LiFAP solutions, solvent reactions such as polymerization may take place, and hence, form resistive surface films (relatively high impedance, Fig. 14). However, these surface films which impede Li-ion transport may better protect the active mass from detrimental interactions with solution species. Thereby, the kinetics of $LiMn_2O_4$

cathodes are more sluggish in LiFAP solutions, but their capacity is higher.

Conclusion

LiFAP solutions in mixtures of commonly used alkyl carbonates such as EC-DMC-DEC were found to be superior to $LiPF_6$ or $LiN(SO_2CF_2CF_3)_2$ solutions for Li-ion batteries. Both Li graphite anodes and $LiMn_2O_4$ cathodes perform better in LiFAP solutions than in the other solutions in terms of higher capacity and lower capacity fading upon cycling. It was also found that both graphite and $LiMn_2O_4$ electrodes are stabilized faster upon repeated lithiation-delithiation cycling in LiFAP solutions than in $LiPF_6$ solutions. The impedance of both graphite and $LiMn_2O_4$ electrodes is higher in LiFAP solutions than in $LiPF_6$ solutions, which makes the kinetics in the former solutions more sluggish. The difference in the behavior of graphite and $LiMn_2O_4$ electrodes in LiFAP and $LiPF_6$ solutions is due to their different surface chemistry in these solutions. In $LiPF_6$ solutions, both unavoidably present HF and the PF_6^- anion, its decomposition product, PF_5, are highly reactive on the electrode surfaces. Consequently, both $LiMn_2O_4$ and graphite electrodes are covered by surface films comprising LiF as a major surface species. Formation of LiF films may inhibit precipitation of surface species originating from solvent reduction products. In the case of LiFAP solutions, the surface chemistry of graphite and $LiMn_2O_4$ electrodes is dominated by reactions of solvent molecules. In the absence of HF contamination, the carbonate species formed by solvent reduction on lithiated graphite electrodes remain stable, and thus form robust passivating surface films. We suggest that the absence of HF and the relatively higher stability and lower reactivity of the FAP^- anion compared with PF_6^- prevent detrimental solution-electrode interactions and allow the development of surface films originating from solvent reactions, that well protect the electrode's active mass.

Acknowledgment

Partial support for this work was obtained from the BMBF, the German Ministry of Science, in the framework of the DIP program for Collaboration Between Israeli and German Scientists.

Bar-Ilan University assisted in meeting the publication costs of this article.

References

1. J. O. Besenhard and M. Winter, *Chem. Phys. Chem.*, **3**, 155 (2002).
2. M. Winter, J. O. Besenhard, M. E. Spahr, and P. Novak, *Adv. Mater.*, **10**, 725 (1998).
3. *Li-Ion Batteries-Fundamentals and Performance*, M. Wakihara and O. Yamamoto, Editors, Kodansha Scientific, Ltd., Tokyo, and Wiley-VCH, Weinheim (1998).
4. M. Broussely, S. Herregre, P. Biensen, P. Kasztejna, K. Nechev, and R. K. Staniewicz, *J. Power Sources*, **97-98**, 13 (2001).
5. M. Broussely, P. Biensan, and B. Simon, *Electrochim. Acta*, **45**, 3 (1999).
6. A. Yamada and S. C. Chung, *J. Electrochem. Soc.*, **148**, A960 (2001).
7. E. Sloop, J. K. Pugh, S. Wang, J. B. Kerr, and K. Kinoshita, *Electrochem. Solid-State Lett.*, **4**, A42 (2001).
8. A. M. Andersson and K. Edstrom, *J. Electrochem. Soc.*, **148**, A1100 (2001).
9. K. Kanamura, S. Shiraishi, and Z. I. Takehara, *J. Electrochem. Soc.*, **143**, 2187 (1996).
10. A. Du Pasquier, A. Blyr, P. Courjal, G. Armatucci, B. Gerand, and J.-M. Tarascon, *J. Electrochem. Soc.*, **146**, 428 (1999).
11. D. Aurbach, B. Markovsky, A. Schechter, Y. Ein-Eli, and H. Cohen, *J. Electrochem. Soc.*, **143**, 3809 (1996).
12. M. Schmidt, U. Heider, A. Kuehner, R. Oesten, M. Jungnitz, N. Ignatev, and P. Sartori, *J. Power Sources*, **97-98**, 557 (2001).
13. D. Aurbach, M. D. Levi, K. Gamolsky, B. Markovsky, G. Salitra, E. Levi, U. Heider, L. Heider, and R. Oesten, *J. Power Sources*, **81-82**, 443 (1999).
14. D. Aurbach, B. Markovsky, M. D. Levi, E. Levi, A. Schechter, M. Moshkovich, and Y. Cohen, *J. Power Sources*, **81-82**, 95 (1999).
15. D. Aurbach, K. Gamolsky, B. Markovsky, G. Salitra, and Y. Gofer, *J. Electrochem. Soc.*, **147**, 1322 (2000).
16. D. Aurbach, M. L. Daroux, P. Faguy, and E. B. Yeager, *J. Electroanal. Chem. Interfacial Electrochem.*, **297**, 225 (1991).
17. D. Aurbach, M. Moshkovich, and Y. Gofer, *J. Electrochem. Soc.*, **148**, E155 (2001).
18. D. Aurbach and A. Zaban, *J. Electroanal. Chem.*, **393**, 43 (1995).
19. K. Kanamura, *J. Power Sources*, **81-82**, 123 (1999).
20. M. Ue, M. Takeda, M. Takehara, and S. Mori, *J. Electrochem. Soc.*, **144**, 2684 (1997).
21. M. D. Levi, E. Levi, and D. Aurbach, *J. Electroanal. Chem.*, **421**, 79,89 (1997).
22. D. Aurbach and M. D. Levi, *J. Phys. Chem. B*, **101**, 4641 (1997).
23. R. Yazami, *Electrochim. Acta*, **45**, 87 (1999).
24. D. Aurbach, A. Zaban, A. Schechter, Y. Ein-Eli, E. Zinigrad, and B. Markovsky, *J. Electrochem. Soc.*, **142**, 2873,2882 (1995).
25. D. Aurbach, A. Schechter, B. Markovsky, Y. Ein-Eli, and V. Koch, *J. Electrochem. Soc.*, **143**, L273 (1996).
26. Y. Ein-Eli, S. F. McDevitt, B. Markovsky, A. Schechter, and D. Aurbach, *J. Electrochem. Soc.*, **144**, L180 (1997).
27. Data base "XI Spec Master," C. Vincent, Editor, XPS International, Kawasaki, Japan (1998).
28. A. Schechter and D. Aurbach, *Langmuir*, **15**, 3334 (1999).
29. K. Kanamura, H. Tamura, S. Shiraishi, and Z. I. Takehara, *J. Electrochem. Soc.*, **142**, 340 (1995).
30. D. Aurbach, B. Markovsky, K. Gamolsky, E. Levi, and Y. Ein-Eli, *Electrochim. Acta*, **42**, 697 (1997).
31. D. Aurbach, Y. Gofer, M. Ben-Zion, and P. Aped, *J. Electroanal. Chem.*, **339**, 451 (1992).
32. V. W. Behrendt, G. Gatlow, and M. Drager, *Z. Anorg. Allg. Chem.*, **397**, 237 (1973).
33. D. Aurbach and E. Granot, *Electrochim. Acta*, **42**, 697 (1997).
34. M. Mokamedi, D. Takahashi, J. Itoh, M. Umeda, and I. Uchida, *J. Electrochem. Soc.*, **149**, A19 (2002).
35. G. Amatucci, A. D. Pasquier, A. Blyr, T. Zheng, and J.-M. Tarascon, *Electrochim. Acta*, **45**, 255 (1999).
36. D. Aurbach, M. D. Levi, E. Levi, H. Teller, B. Markovsky, G. Salitra, L. Heider, and U. Heider, *J. Electrochem. Soc.*, **145**, 3024 (1998).
37. K. Kanamura, T. Umegaki, M. Ohashi, S. Toriyama, S. Shiraishi, and Z. I. Takehara, *Electrochim. Acta*, **47**, 433 (2001).